Algorithmic optimization of quantum optical storage in solids

Yisheng Lei,[1] Haechan An,[1,2] Zongfeng Li,[1] and Mahdi Hosseini[1,2,*]

[1]Department of Electrical and Computer Engineering and Applied Physics Program, Northwestern University, Evanston, Illinois 60208, USA
[2]Elmore Family School of Electrical and Computer Engineering, Purdue University, West Lafayette, Indiana 47907, USA

(Received 5 April 2024; accepted 29 July 2024; published 9 August 2024)

Quantum memory devices with high storage efficiency and bandwidth are essential elements for future quantum networks. Solid-state quantum memories can provide broadband storage, but they primarily suffer from low storage efficiency. We use passive optimization and algorithmic optimization techniques to demonstrate nearly a sixfold enhancement in quantum memory efficiency. In this regime, we demonstrate coherent and single-photon-level storage with a high signal-to-noise ratio. The optimization technique presented here can be applied to most solid-state quantum memories to significantly improve the storage efficiency without compromising the memory bandwidth.

DOI: 10.1103/PhysRevResearch.6.033153

I. INTRODUCTION

Rare-earth-ion doped solids have been attractive platforms for the development of quantum optical memories [1]. The atomic frequency comb technique [2] has become the primary storage protocol in solids due to its broadband and low-noise properties. Typically, a two-pulse train pumping sequence is used to perform spectral tailoring and create an atomic frequency comb (AFC) [3,4]. Improving optical depth using impedance-matched resonators can be used to improve storage efficiency at the expense of lowering the memory bandwidth [5,6]. Optimizing the pumping and preparation sequence is also crucial for better spectral tailoring leading to higher storage efficiency. In the case of laser-cooled atoms, machine-learning optimization has been deployed to enhance atom trapping and cooling [7,8]. Such optimization has not been explored in the context of solid-state quantum memories. In this article, we perform machine-learning optimization based on a genetic algorithm for AFC quantum storage in a Tm^{3+}:YAG crystal. Tm^{3+} ions in solids have optical transition wavelengths close to those of rubidium atoms, making them good candidates for building hybrid quantum networks [9]. Many experiments are performed using Tm^{3+}:YAG crystal [3,10], as well as Tm^{3+}:YGG crystal [11,12], Tm^{3+}:$LiNbO_3$ crystal [13,14], and Tm^{3+} ions doped in lithium niobate on insulator [15]. Tm^{3+} ions in YAG crystal have a long optical coherence time of 100 μs, a ground-state lifetime of over 1 s at around 1 K, and a high branching ratio of 25% [16], making it a good system for spectral tailoring for photon storage. Our experiment is carried out using a tabletop cryostat at 3.5 K and a magnetic field produced by a compact permanent magnet. We first passively enhance the optical depth without compromising bandwidth by routing the laser beam multiple times through the crystal. We then run a genetic algorithm to design a more efficient spectral preparation sequence. We show that the combination of these techniques can lead to a significant improvement in storage efficiency. We also demonstrate coherent and single-photon-level storage with a high signal-to-noise ratio.

II. EXPERIMENTAL RESULTS AND ANALYSIS

The experimental setup is shown in Fig. 1(a). The Tm^{3+}:YAG crystal with dimensions $4 \times 5 \times 10$ mm (crystal axis $\langle 001 \rangle$, $\langle 1\bar{1}0 \rangle$, and $\langle 110 \rangle$) has a doping concentration of 0.1%. The laser beam (Toptica DL Pro) propagates parallel to the $\langle 110 \rangle$ axis with linear polarization ($E \parallel \langle 1\bar{1}0 \rangle$ axis). The optical transition $^3H4 \leftrightarrow {}^3H6$ occurs at a wavelength of $\lambda = 793.373$ nm. A permanent magnet produces a magnetic field of 600 G along the $\langle 001 \rangle$ axis, lifting the degeneracy of Tm^{3+} ions with a nuclear spin of 1/2. One of the two ground states can serve as a shelving state for spectral preparation. With spectral hole burning, its hole and sideholes (due to inhomogeneous broadening) are separated by 3.75 MHz, indicating that the excited state is split by 3.75 MHz and the ground-state splitting is determined to be 17.3 MHz. The two-pulse echo technique is used to measure the homogeneous linewidth. The echo intensities are measured with different time separations between the two pulses, where an exponential fitting outputs a maximum coherence time of 60 μs, which is inverse of the homogeneous linewidth. Additional measurements of spectral hole decay with double-exponential fitting output a fast decay lifetime of 10 ms and a slow decay lifetime of 110 ms, corresponding to the intermediate level $^3F_4$ lifetime and the ground-state lifetime [17].

We implement an AFC protocol for storage, which relies on spectral tailoring and atomic rephasing [2]. A common approach for spectral tailoring is to use a two-pulse train to optically pump atoms into an AFC. We first implement AFC using two identical Gaussian pulses of width 50 ns separated by $t_s = 200$ ns with a 5 μs delay between pulse pairs, repeated

*Contact author: mh@northwestern.edu

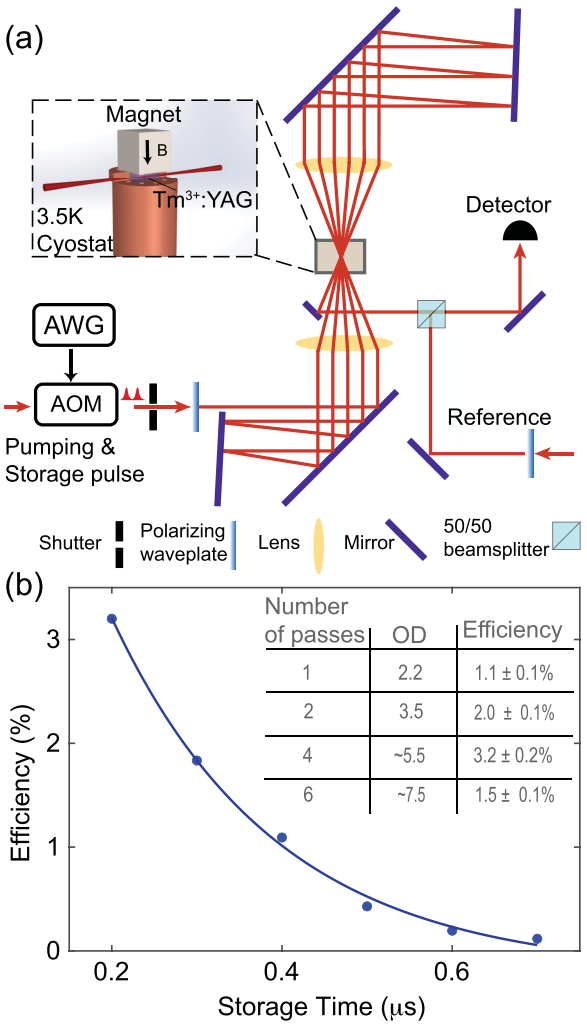

FIG. 1. (a) Experimental setup is shown where a Tm^{3+}:YAG crystal is placed inside a 3.5 K cryostat below a permanent magnet. A few mirrors (M) are used to direct the optical signal to pass multiple times through the crystal. For interferometric detection, the signal is interfered with a reference light with 80 Hz frequency difference. AOM: acousto-optic modulator; AWG: arbitrary waveform generator. (b) Results of multipass two-pulse train atomic frequency comb (AFC) storage. Four-pass echo efficiency is plotted as a function of the time separations between the two pulses used to create AFC. An exponential fit with a time constant of 194 ns indicates the storage time. The inset shows the echo efficiency and the estimated optical depth for different numbers of passes through the memory with a storage time of 200 ns.

15 000 times followed by a 20 ms wait time. A 50 ns weak coherent pulse is then sent to carry out storage. This approach gives rise to a memory bandwidth of 20 MHz, a storage time of $t_s = 200$ ns, and a memory efficiency of $1.1 \pm 0.1\%$.

The AFC memory efficiency ideally scales with optical depth (OD) as [18]

$$\eta = \frac{d^2}{F^2}\exp\left(-\frac{d}{F}\right)\exp\left(-\frac{1}{F^2}\frac{\pi^2}{4\ln 2}\right)\exp(-d_0), \qquad (1)$$

where d is the OD of the atomic medium, F is the finesse of the comb, and d_0 is the total background absorption. Finesse is defined as the ratio between the spacing and width of the Gaussian comb lines. The typical finesse of a frequency comb produced by a two-pulse-train pump is around 2–3. In the case of an ideal Gaussian-teeth AFC, the maximum storage efficiency can be achieved with an OD of 4–6. Increasing the optical depth can be achieved simply by using a longer crystal, but it would require more cooling power and a larger sample space in the cryostat. In our experiment, we first route the laser beam to pass through the crystal multiple times. For different numbers of passes, both echo efficiency and OD are measured [see Fig. 1(b)]. Maximum efficiency was observed for the four-pass configuration. At higher numbers of passes, storage efficiency drops because the pumping laser intensity and time are limited by laser heating and ground-state lifetime, respectively. We also observe that the OD does not show a linear relationship with the number of passes, which we attribute to the nonzero overlap between different beam paths. The efficiency relationship in Eq. (1) assumes a simple atomic level structure and an infinite comb with perfect Gaussian teeth. In practice, the experimental effects of optoelectronic devices, optical and electronic delays, and the complex atomic-level structure can cause deviations from predictions obtained through a straightforward Fourier transform of the ideal pumping pulse train in the time domain. Machine learning optimization can offer significant benefits in addressing these complexities. Thus, to further improve the pumping and storage efficiency for the four-pass configuration, we employ machine learning based on a genetic algorithm. Genetic algorithms and their variants are recognized as derivative-free optimization algorithms capable of delivering high-quality solutions even with straightforward implementation. This makes genetic algorithms attractive optimization tools in various fields, including atomic and optical experiments [19–22]. The genetic algorithm is inspired by the theory of natural evolution and its flow is schematically shown in Fig. 2(a). Individuals have a genetic code consisting of parameters to be optimized. Each individual is evaluated on how close it is to the optimization goal and individuals with good evaluation results (fitness) are selected to create the next generation. The genetic codes of offspring are made by crossing over and mutating the parents' genetic code. Keeping the individuals with the best fitness (elites) to the next generation can accelerate the optimization. Repeating this process for several generations leads to the evolution of individuals and delivers solutions to an optimization problem. We send the same 50 ns pulse as an input signal to AFC memory, use the first echo intensity as the fitness function, and employ the genetic algorithm to optimize pulse parameters as shown in Fig. 2(a). We note that employing echo intensity, or equivalently, memory efficiency, as the cost function, ensures optimal memory performance for a specific memory bandwidth (determined by input pulse bandwidth) at a given storage time. We first consider a two-pulse pumping sequence and set the pulse widths ($t_p = 20$–100 ns), amplitudes ($P =$ 0–0.6 V, corresponding to approximately 0–10 mW) laser output, loop duration ($T_d = 2$–10 μs), and the number of loops ($N = 5$k–50k) as constrained variables, while keeping pulse separations fixed at $t_s = 200$ ns. We set both the total number of generations and population to 20. Parents are selected through tournament selection with a tournament size of 10.

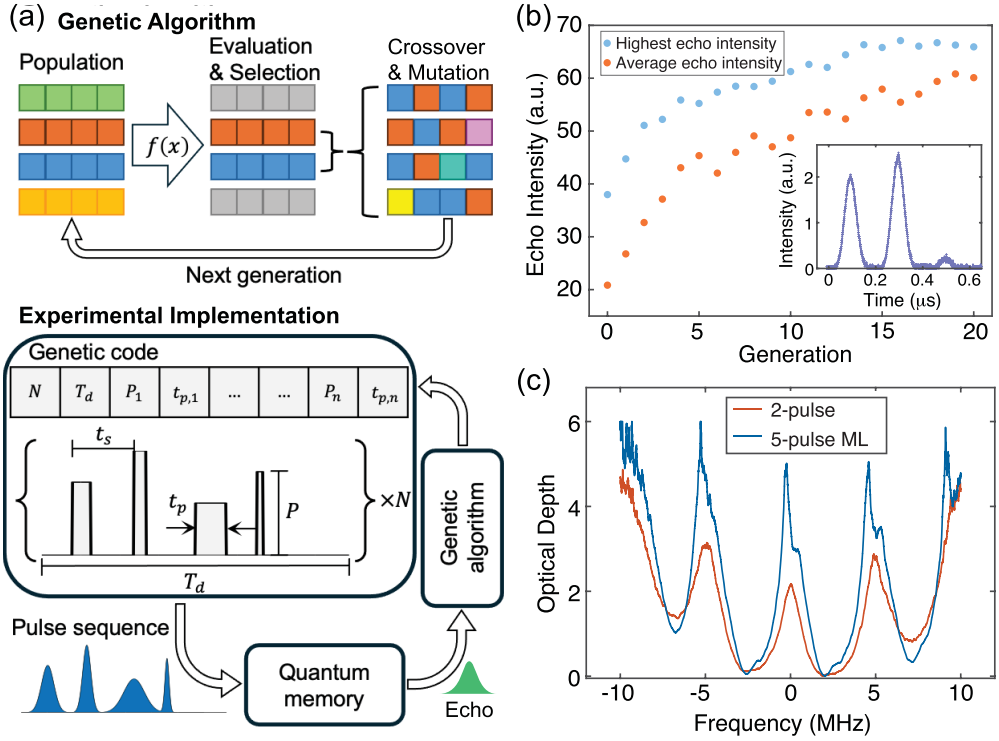

FIG. 2. (a) Flow diagram of the genetic algorithm (top) and its implementation in atomic frequency comb memory (bottom). The genetic algorithm evaluates parameter sets and generates the next parameter set from the current parameter sets and their evaluation results. Repetition of this evolution of parameter sets leads to sets with good evaluation results. In the context of atomic frequency comb memory, the parameters to be optimized are the design parameters of the pumping pulse sequence, while the evaluation and results focus on the efficiency of the atomic frequency comb memory and the echo. (b) The mean and best value of echo intensity for every generation of the genetic algorithm is plotted. The inset figure is an example of classical echo intensity measurement used for this optimization. The first peak is the unabsorbed transmission of the input pulse, the second peak is the first echo, and the third peak is the second echo. (c) Optical depth after pumping is plotted as a function of relative frequency for the traditional two-pulse-train pumping sequence and an optimized five-pulse sequence.

Three elites are kept to the next generation. The AFC pumping results in a bandwidth of around 20 MHz corresponding to the bandwidth of the 50 ns input data pulse. However, fine-tuning the bandwidth, AFC contrast, and finesse of the AFC, as well as the pumping duration, are subjects of the optimization process, for which five parameters were chosen. The process can be repeated for any input temporal shape. We note that a larger memory bandwidth requires higher pumping power and longer pumping time, whereas a smaller memory bandwidth relative to the input pulse bandwidth necessitates shorter and weaker pumping. While this latter scenario is desirable, it also leads to lower memory efficiency. Hence the optimization algorithm is valuable in balancing these trade-offs.

Figure 2(b) shows the best and mean fitness of each generation, with fitness improving over generations. The small fluctuation in the best fitness is due to the fluctuation of the echo intensity for each measurement. The fluctuation in the experimental result directly affects optimization and becomes the resolution of optimization. We reduce fluctuation by averaging 25 echo measurements and apply Gaussian fitting to find echo intensity as a measure of efficiency. We then consider n-pulse train sequences with $n = 1$–10 and identify the five-pulse sequence to be the most optimum with a memory efficiency of $6.4 \pm 0.1\%$, which is a 100% increase compared to simple two-pulse-train pumping. The optimal pulse parameters are found to be $P, t_p =$ (0.11 V, 21 ns; 0.10 V, 55 ns; 0.31 V, 60 ns; 0.51 V, 67 ns; 0.10 V, 62 ns), with a loop duration $T_d = 4.2$ μs and $N = 45,600$ loops. As seen in Fig. 2(c), the optimized pumping sequence results in less background absorption and a higher optical depth. The comb finesse $F = 3.68$, optical depth $d \sim 5$, and optical background absorption $d_0 \sim 1.5$, which should result in a theoretical efficiency of 8.1% based on Eq. (1). We attribute this slight discrepancy to the imperfect comb shape and finite comb length. We also tried more complicated sequences, such as multistage pumping (running a few different pulse sequences sequentially), but it did not yield better results.

We also carry out interferometric measurements and evaluate the optimized output performance using the coherent echo amplitude as the fitness. The amplitude of the echo measured in this way is sensitive to phase noise. Due to the increased measurement sensitivity, optimization can be applied to relatively weak pulses to avoid potential saturation and confirm the best pumping protocol. We interfere the weak storage pulse with a reference light of 80 MHz frequency difference on a 50:50 beam splitter. The amplitude of the interference envelope is set as the fitness and the algorithmic optimization outputs a pumping sequence with a memory efficiency increase of 80% compared to the simple two-pulse pumping.

We also perform single-photon level storage using an attenuated coherent pulse and a mechanical shutter to fully block the pumping beam during storage. After each spectral

preparation and 20 ms waiting, 100 weak storage pulses separated by 10 μs are sent to the crystal. A semiconductor avalanche single photon detector with an efficiency of 60% (Laser Components, Single Photon Counting Module) is turned on for 2 μs for every storage pulse to record its transmission and echo pulses. In total, 10 000 storage events are performed and measured. Single photon measurements with five different average input photon numbers have been performed. Average photon numbers of the first echo range from 0.02 to 0.3. The input storage pulse intensities are measured by tuning the laser frequency off-resonant and adding a neutral density filter to reduce its intensity to 5%, as shown in Fig. 3(b). A memory efficiency of $5.5 \pm 0.1\%$ for the optimized five-pulse pumping sequence is measured and $3.0 \pm 0.1\%$ for the simple two-pulse sequence. In the case of two-pulse-train pumping, the resulting less-than-ideal AFC structure leads to dispersion [23] of the leakage light (unabsorbed pulse, depicted in red). By measuring the variance of single-photon detection events [Fig. 3(c)], we confirm that the noise of the echo signal is shot-noise limited, i.e., $\mathrm{Var}(n_{\mathrm{ph}}) \simeq \langle n_{\mathrm{ph}} \rangle$, complementing the coherent storage results from interferometric measurement.

III. DISCUSSION

We note that storage efficiency is not directly correlated with signal-to-noise ratio, which can be affected by intensity of the input storage pulse. The three different measurements of intensity detection of strong classical pulses, amplitude detection (interferometric measurement) of weak classical pulses, and single-photon detection of weak coherent pulses differ in the type of information they provide. At high intensity, saturation could play a role. On the other hand, measuring intensity or photon counting at high or low powers, respectively, does not measure the phase and simply leads to optimization of the echo intensity. Interferometric detection measures amplitude and is sensitive to phase noise. Moreover, it is conducted at relatively low powers where saturation is not present. Since optimization via single-photon detection is difficult and time consuming, we carried out the optimization for intensity and interferometric detection to see if there is a difference in performance at the single-photon level. The fact that the two processes yield similar results at the single-photon level is an indication of unbiased optimization.

To further improve efficiency, moderate modifications are needed to increase the finesse of the AFC and reduce the background absorption. As shown previously, this can be achieved by reducing the laser linewidth and crystal temperature [24]. In our experiment, the laser linewidth and the ground-state lifetime of Tm^{3+} ions limit the performance of spectral tailoring. Frequency locking of the laser can reduce the spectral linewidth and lower temperature can prolong the ground-state lifetime. Further reducing the cryostat's vibrations will help to run more sophisticated genetic algorithms with faster and more accurate optimizations. Combining our proof-of-concept optimization with these improvements, the comb finesse $F = 4$–5, optical depth $d \sim 8$ (in a six-pass configuration), and optical background absorption $d_0 \sim 0.1$ can be achieved, resulting in an efficiency of ~40% without compromising storage bandwidth. This is already very close to the maximum AFC efficiency expected in the case of forward retrieval, which is 54% [18]. Cavity impedance matching conditions are another way to increase memory

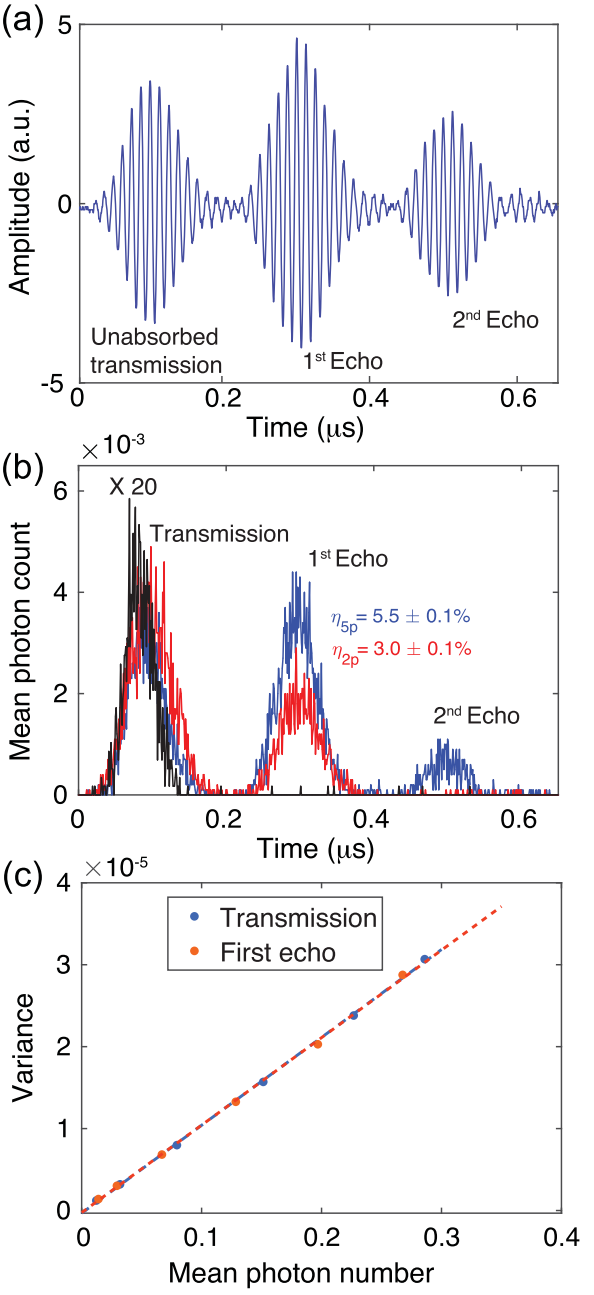

FIG. 3. (a) Interferometric measurement of memory output for the optimized five-pulse sequence is plotted, indicating the coherent nature of the storage. (b) Single-photon level storage is presented where the black curve represents the input storage pulse measured by tuning the laser frequency off-resonant, while the signal in blue and red represents the memory outgoing signal obtained from the optimized five-pulse pumping sequence and the two-pulse-train pumping sequence, respectively. (c) The variance of the photon number for the first echo and leakage pulses is plotted against the average photon number of the first echo, obtained from 10^4 storage events. Linear fittings (blue and red dashed lines) output slopes of $1.073/10^4$ and $1.068/10^4$ for transmission and first echo pulses, respectively, in agreement with the expected shot-noise limit.

efficiency [10], albeit at the expense of lowering the memory bandwidth. Narrow laser spectral linewidth will also help to prepare a comb with smaller Δ, which will give a longer storage time. Other pumping sequences such as the intrinsic pumping method [12] can be employed to enhance the memory bandwidths up to $\sim$10 GHz.

IV. CONCLUSION

In conclusion, we demonstrate that by optimizing effective OD via multipass configuration and employing optimization-algorithm-assisted memory preparation, the efficiency of quantum optical storage can increase by about a factor of 6 in a Tm^{3+}:YAG crystal. We conduct classical, coherent, and single-photon-level storage to compare optimization results and characterize quantum noise. Our findings indicate that classical algorithmic optimization can significantly enhance quantum storage performance without introducing intensity or phase noise to the system. This method is applicable to other storage protocols developed in various rare-earth solids.

Data underlying the results presented in this paper are not publicly available at this time but may be obtained from the authors upon reasonable request.

ACKNOWLEDGMENTS

We acknowledge the support from National Science Foundation CAREER Award No. 2410198 and U.S. Department of Energy, Office of Science, Office of Advanced Scientific Computing Research, through the Quantum Internet to Accelerate Scientific Discovery Program under Field Work Proposal No. 3ERKJ381.

The authors declare no conflicts of interest.

[1] Y. Lei, F. K. Asadi, T. Zhong, A. Kuzmich, C. Simon, and M. Hosseini, Quantum optical memory for entanglement distribution, Optica **10**, 1511 (2023).

[2] M. Afzelius, C. Simon, H. de Riedmatten, and N. Gisin, Multimode quantum memory based on atomic frequency combs, Phys. Rev. A **79**, 052329 (2009).

[3] T. Chanelière, J. Ruggiero, M. Bonarota, M. Afzelius, and J. Le Gouët, Efficient light storage in a crystal using an atomic frequency comb, New J. Phys. **12**, 023025 (2010).

[4] M.-H. Jiang, W. Xue, Q. He, Y.-Y. An, X. Zheng, W.-J. Xu, Y.-B. Xie, Y. Lu, S. Zhu, and X.-S. Ma, Quantum storage of entangled photons at telecom wavelengths in a crystal, Nat. Commun. **14**, 6995 (2023).

[5] M. Afzelius and C. Simon, Impedance-matched cavity quantum memory, Phys. Rev. A **82**, 022310 (2010).

[6] S. A. Moiseev, S. N. Andrianov, and F. F. Gubaidullin, Efficient multimode quantum memory based on photon echo in an optimal QED cavity, Phys. Rev. A **82**, 022311 (2010).

[7] A. D. Tranter, H. J. Slatyer, M. R. Hush, A. C. Leung, J. L. Everett, K. V. Paul, P. Vernaz-Gris, P. K. Lam, B. C. Buchler, and G. T. Campbell, Multiparameter optimisation of a magneto-optical trap using deep learning, Nat. Commun. **9**, 4360 (2018).

[8] Z. Vendeiro, J. Ramette, A. Rudelis, M. Chong, J. Sinclair, L. Stewart, A. Urvoy, and V. Vuletić, Machine-learning-accelerated Bose-Einstein condensation, Phys. Rev. Res. **4**, 043216 (2022).

[9] F. Gu, S. G. Menon, D. Maier, A. Das, T. Chakraborty, W. Tittel, H. Bernien, and J. Borregaard, Hybrid quantum repeaters with ensemble-based quantum memories and single-spin photon transducers, arXiv:2401.12395.

[10] J. H. Davidson, P. Lefebvre, J. Zhang, D. Oblak, and W. Tittel, Improved light-matter interaction for storage of quantum states of light in a thulium-doped crystal cavity, Phys. Rev. A **101**, 042333 (2020).

[11] C. W. Thiel, N. Sinclair, W. Tittel, and R. L. Cone, Tm^{3+} : $Y_3Ga_5O_{12}$ materials for spectrally multiplexed quantum memories, Phys. Rev. Lett. **113**, 160501 (2014).

[12] M. F. Askarani, A. Das, J. H. Davidson, G. C. Amaral, N. Sinclair, J. A. Slater, S. Marzban, C. W. Thiel, R. L. Cone, D. Oblak *et al.*, Long-lived solid-state optical memory for high-rate quantum repeaters, Phys. Rev. Lett. **127**, 220502 (2021).

[13] N. Sinclair, E. Saglamyurek, H. Mallahzadeh, J. A. Slater, M. George, R. Ricken, M. P. Hedges, D. Oblak, C. Simon, W. Sohler *et al.*, Spectral multiplexing for scalable quantum photonics using an atomic frequency comb quantum memory and feed-forward control, Phys. Rev. Lett. **113**, 053603 (2014).

[14] M. F. Askarani, J. H. Davidson, V. B. Verma, M. D. Shaw, S. W. Nam, T. Lutz, G. C. Amaral, D. Oblak, W. Tittel *et al.*, Entanglement and nonlocality between disparate solid-state quantum memories mediated by photons, Phys. Rev. Res. **2**, 013039 (2020).

[15] S. Dutta, Y. Zhao, U. Saha, D. Farfurnik, E. A. Goldschmidt, and E. Waks, An atomic frequency comb memory in rare-earth-doped thin-film lithium niobate, ACS Photon. **10**, 1104 (2023).

[16] A. Louchet, J. S. Habib, V. Crozatier, I. Lorgeré, F. Goldfarb, F. Bretenaker, J.-L. Le Gouët, O. Guillot-Noël, and P. Goldner, Branching ratio measurement of a Λ system in Tm^{3+}: YAG under a magnetic field, Phys. Rev. B **75**, 035131 (2007).

[17] N. Sinclair, D. Oblak, E. Saglamyurek, R. L. Cone, C. W. Thiel, and W. Tittel, Optical coherence and energy-level properties of a Tm^{3+}-doped $LiNbO_3$ waveguide at subkelvin temperatures, Phys. Rev. B **103**, 134105 (2021).

[18] B. Lauritzen, J. Minář, H. de Riedmatten, M. Afzelius, and N. Gisin, Approaches for a quantum memory at telecommunication wavelengths, Phys. Rev. A **83**, 012318 (2011).

[19] R. S. Judson and H. Rabitz, Teaching lasers to control molecules, Phys. Rev. Lett. **68**, 1500 (1992).

[20] T. Hornung, R. Meier, D. Zeidler, K.-L. Kompa, D. Proch, and M. Motzkus, Optimal control of one- and two-photon transitions with shaped femtosecond pulses and feedback, Appl. Phys. B **71**, 277 (2000).

[21] Y. Chen, C. Wang, Y. Yu, Z. Jiang, J. Wang, S. Zhao, D. Wei, H. Gao, and F. Li, Genetic algorithm optimization for storing arbitrary multimode transverse images in thermal atomic vapor, Appl. Phys. Lett. **118**, 234001 (2021).

[22] E. Robertson, L. Esguerra, L. Messner, G. Gallego, and J. Wolters, Machine learning optimal control pulses in an optical quantum memory experiment, arXiv:2401.05077.

[23] M. Bonarota, J. Le Gouët, S. Moiseev, and T. Chaneliere, Atomic frequency comb storage as a slow-light effect, J. Phys. B: At., Mol., Opt. Phys. **45**, 124002 (2012).

[24] P. Jobez, N. Timoney, C. Laplane, J. Etesse, A. Ferrier, P. Goldner, N. Gisin, and M. Afzelius, Towards highly multimode optical quantum memory for quantum repeaters, Phys. Rev. A **93**, 032327 (2016).